Impulsive and Low-Thrust Transfer Design Between Stable and Nearly-Stable Periodic Orbits in the Restricted Problem

Conference Paper · January 2018

DOI: 10.2514/6.2018-1690

3 authors:

Robert Pritchett
Purdue University
1 PUBLICATION **0** CITATIONS
SEE PROFILE

Emily Zimovan
Purdue University
4 PUBLICATIONS **14** CITATIONS
SEE PROFILE

Kathleen Howell
Purdue University
201 PUBLICATIONS **2,757** CITATIONS
SEE PROFILE

Impulsive and Low-Thrust Transfer Design between Stable and Nearly-Stable Periodic Orbits in the Restricted Problem

Robert E. Pritchett,* Emily M. Zimovan, † and Kathleen C. Howell ‡
Purdue University, 701 West Stadium Avenue, West Lafayette, IN 47907-2045

Wide-ranging transfer capabilities are necessary to support the development of cislunar space. But, the design of efficient low-thrust and impulsive transfers between stable periodic orbits is challenging in this regime. Transfer concepts between such orbits cannot leverage the unstable manifold structures typically employed. Thus, a methodology for constructing such transfers, based on collocation, is demonstrated. Initial guesses comprised of coast arcs along periodic orbits as well as "chains" of intermediate trajectory arcs from other natural dynamical structures are exploited to yield optimal transfers. Optimal low-thrust transfers are transitioned to impulsive trajectories or continued to introduce practical engine parameters. This process applies to various spacecraft configurations and some results are validated in a higher-fidelity model. Practical examples demonstrate direct transcription as a robust approach for constructing low-thrust transfers.

I. Nomenclature

m_1	=	mass of the larger primary in the CR3BP
m_2	=	mass of the secondary in the CR3BP
μ	=	mass ratio of the primary bodies in the CR3BP
x, y, z	=	Cartesian position components corresponding to the third body in the CR3BP
d	=	distance from the larger primary to the third body in the CR3BP
r	=	distance from the secondary to the third body in the CR3BP
v	=	velocity magnitude for the third body in the CR3BP relative to the rotating frame
Δv	=	change in velocity magnitude
θ	=	nondimensional angular velocity of the rotating frame with respect to the inertial frame in the CR3BP
U	=	pseudo-potential function in the CR3BP
J	=	Jacobi constant value
J_0, J_f	=	Jacobi constant value of departure (0) and arrival (f) orbits in a transfer
m_q	=	mass of the central body in an N-body model
m_i	=	mass of the particle of interest in an N-body model
m_j	=	mass of the additional perturbing bodies in an N-body model
$\boldsymbol{p}_{qi}$	=	three element state vector from body q to body i comprised of position components in the inertial frame
G	=	universal gravitational constant
m_0, m_f	=	initial (0) and final (f) spacecraft mass
v_e	=	exhaust velocity
g_0	=	acceleration due to gravity at the surface of the Earth
T_{max}	=	maximum thrust of a low-thrust engine
I_{sp}	=	specific impulse of a low-thrust engine
n	=	number of patch points/nodes used to discretize a trajectory
η_k	=	number or orbit revolutions stacked on a single link k of an orbit chain
r_p	=	radius of periapse
A_z	=	maximum positive Z amplitude of a halo orbit

*Ph.D. Student, School of Aeronautics and Astronautics, pritcher@purdue.edu, AIAA Student Member.
†Ph.D. Student, School of Aeronautics and Astronautics, ezimovan@purdue.edu, AIAA Student Member.
‡Hsu Lo Distinguished Professor of Aeronautics and Astronautics, School of Aeronautics and Astronautics, howell@purdue.edu, AIAA Fellow.

II. Introduction

The establishment of a permanent human presence in cislunar space is a near term goal of both government space agencies and private companies. This objective will enable the advancement of scientific knowledge through the creation of facilities in lunar orbit to serve as departure points for missions to explore the Moon, Mars, and beyond. Furthermore, it will facilitate the formation of a productive space economy beyond low-Earth orbit. A sample implementation toward this ambitious goal is the Deep Space Gateway (DSG), a crewed lunar space station concept presently being investigated by NASA in partnership with several other space agencies [1]. United Launch Alliance (ULA) also seeks to make this vision a reality with the development of a cislunar infrastructure [2]. These and other concepts for installing an enduring human presence in cislunar space will be aided by exploiting a variety of stable and nearly stable periodic orbits in the Earth-Moon system. The natural stability of these orbits enables a spacecraft to remain in orbit there with relatively low propellant expenditures. Thus, these trajectories are well-suited for communications spacecraft, space stations and propellant depots, among other applications. Given their utility, there is a crucial need for the development of transfers to and between these orbits, for both high-thrust crewed spacecraft and low-thrust cargo vehicles. Transfer scenarios between lunar orbits of varying geometries, enabled by powerful ion engines, are already under consideration for the DSG concept. Therefore, the investigation into effective design techniques for these types of transfers is motivated by the impending requirements.

While the development of cislunar space implies that stable periodic orbits near the Moon, such as Near Rectilinear Halo Orbits (NRHOs) or Distant Retrograde Orbits (DROs), offer increasing utility, transfer design between these types of orbits presents distinct challenges. Because the natural dynamical motion often leveraged to guide transfer design (i.e., stable and unstable manifolds) is less prominent, extremely slow, or simply absent near stable orbits, the priority is a set of additional techniques to construct transfers that possess reasonable propellant costs and times of flight. Numerous authors have investigated strategies for designing impulsive and low-thrust transfers from the Earth to particular stable and nearly stable periodic orbits in the Earth-Moon system; [3–6] yet, fewer investigations of general strategies for transfers between such orbits are available. Notable examples include the work by Capdevila et al. to generate a network of impulsive transfers between stable periodic orbits in the Earth-Moon system, including DROs and NRHOs [7]. Parker et al. [8] construct low-thrust transfers from Earth to DROs, as does Herman [9] who also develops transfers between DROs. Low-thrust transfers from L_2 halo orbits to DROs are computed by Parrish et al. [10], however, the type of halo orbits examined are beyond the range presently characterized as NRHOs. Finally, Lantoine [11] investigates transfers from NRHOs to DROs that travel far outside the Earth-Moon system such that perturbations from the Sun aid the design of highly efficient transfers. A similar review of the relevant literature is offered by Pritchett, Howell, and Grebow [12].

In response to the lack of a general algorithm, this investigation seeks to develop a framework for computing impulsive and low-thrust transfers between a variety of orbits in the Earth-Moon system, with a special focus on stable periodic orbits. In particular, a direct transcription algorithm that utilizes "chains" of natural dynamical structures beyond the inherent manifolds is detailed as a favorable strategy for producing initial guesses for successful transfers. Additionally, a paradigm to transition trajectory solutions between low-thrust and impulsive engine models and vice versa is detailed. Applications in the current investigation demonstrate that the methodology is suitable for designing low-thrust and impulsive transfers between periodic orbits in the Earth-Moon system, and that this approach is especially effective when little information is available for developing an initial guess *a priori*.

III. Background and Formulation

The dynamical model and the numerical tools that are leveraged to execute the proposed methodology are detailed along with the process for orbit chain construction. A simplified three-body model that offers a diverse array of natural dynamical structures for use in an orbit chain is described, as well as a higher fidelity N-body model based on ephemeris data. Two different numerical schemes for generating continuous spacecraft trajectories are also outlined. A direct transcription method is well-suited for computing optimal low-thrust trajectories and implementing an orbit chaining approach, while a multiple shooting algorithm is convenient for computing impulsive transfer trajectories. Finally, the procedure for selecting the links in an orbit chain and assembling these components into an initial guess for the direct transcription algorithm is introduced.

A. Dynamical Models

1. The Circular Restricted Three-Body Problem

The circular restricted three-body problem (CR3BP) is the primary dynamical model employed for concept development in this investigation. The CR3BP incorporates the gravitational impact of two massive bodies, for example, the Earth and Moon, on the motion of a third body that is assumed to be massless, e.g., a spacecraft. The two massive bodies are assumed to be in a circular Keplerian orbit about their barycenter, and the mass ratio, $\mu = m_2/(m_1 + m_2)$, characterizes the CR3BP system. Additionally, a rotating coordinate system, is defined based on the motion of the primaries such that the $\hat{x}$ axis is directed along the line joining the two primaries from the more to the less massive body. The $\hat{z}$ axis is aligned with the angular velocity vector of the primary orbit, and the $\hat{y}$ axis completes the orthonormal set. To facilitate numerical computation, the states in the CR3BP are typically nondimensionalized using characteristic quantities. The characteristic length, l^*, equals the distance between the primaries, while the characteristic time, t^*, is selected such that the magnitude of the nondimensional angular velocity of the primaries, θ, is equal to one. The equations of motion governing the motion of the third body are then,

$$\ddot{x} - 2\theta\dot{y} - \theta^2 x = -\frac{(1-\mu)(x+mu)}{d^3} - \frac{\mu(x-1+\mu)}{r^3} \tag{1}$$

$$\ddot{y} + 2\theta\dot{x} - \theta^2 y = -\frac{(1-\mu)y}{d^3} - \frac{\mu y}{r^3} \tag{2}$$

$$\ddot{z} = -\frac{(1-\mu)z}{d^3} - \frac{\mu z}{r^3} \tag{3}$$

where d and r are the distances between the third body and each of the primaries, i.e., $d = \sqrt{(x-\mu)^2 + y^2 + z^2}$ and $r = \sqrt{(x-1+\mu)^2 + y^2 + z^2}$. Additionally, the CR3BP possesses one constant of the motion, denoted the Jacobi constant, J, and defined by the expression, $J = 2U - v^2$, where v is velocity magnitude representing the motion of the third body relative to the rotating frame and U is the pseudo-potential function. The Jacobi constant is an energy-like quantity that is convenient for characterizing various natural dynamical structures in the CR3BP. By exploiting the natural dynamical flow present in this model, low-energy trajectories are enabled. Thus, the use of the CR3B model avoids the increased complexity inherent in a full ephemeris model due to time dependence and additional perturbations. Once a suitable transfer is constructed, the result is transitioned to a higher-fidelity model that maintains the desirable transfer characteristics.

The modeling of low-thrust spacecraft trajectories requires that specific spacecraft and engine parameters also be defined. In this investigation, parameters corresponding to two different spacecraft types are employed. First, a smaller spacecraft model, with initial mass, $m_0 = 1,000\ kg$, and maximum thrust, $T_{max} = 200\ mN$, is examined. Second, a spacecraft model with $m_0 = 40\ mT$ and $T_{max} = 1.2\ N$ is introduced; these characteristics are consistent with the types of engines under consideration for larger low-thrust spacecraft such as the proposed Deep Space Gateway concept [13, 14]. Note that both of these spacecraft models are employed with a specific impulse, $I_{sp} = 2000\ sec$. Because initial mass and maximum thrust values are generally spacecraft dependent, comparison between low-thrust systems is simplified by considering the ratio of thrust-to-mass for each system, i.e., the maximum acceleration a spacecraft can impart. Table 1 summarizes the acceleration levels of the two low-thrust systems in this analysis as well as other representative low-thrust spacecraft. Additionally, to aid comparison between low-thrust and impulsive solutions the equivalent Δv associated with each low-thrust transfer computed in this investigation is calculated with the familiar rocket equation,

$$\Delta v = v_e \ln \frac{m_0}{m_f} \tag{4}$$

where v_e is the exhaust velocity as defined, $v_e = g_0 I_{sp}$. Also, m_f is the final mass of the spacecraft at the completion of the transfer, and g_0 is the acceleration due to gravity at the surface of the Earth, $g_0 = 9.80665\ m/s^2$. Finally, while only two types of low-thrust systems are examined here, the methodology is applicable to a wide range of spacecraft configurations.

2. The Ephemeris Model

While the CR3BP is suitable for the initial phases of the trajectory design process, a higher fidelity model must be employed to validate a trajectory before it can be employed in realistic mission scenarios. This investigation employs N-body equations of motion along with planetary ephemerides to create a high-fidelity dynamical model for the

Table 1 Representative low-thrust spacecraft acceleration levels.

Spacecraft	Max Acceleration (m/s^2)
Small Model	2×10^{-4}
Deep Space 1 [15]	1.892×10^{-4}
Dawn [16]	7.473×10^{-5}
Hayabusa [17]	4.706×10^{-5}
Large Model	3×10^{-5}

validation of impulsive trajectories. Formation of an ephemeris model begins with the definition of an inertial reference frame. Conventionally, the reference frame is centered at one of the bodies included in the ephemerides whose mass is denoted m_q, while another of these bodies is selected as the particle of interest with mass, m_i. The path of the particle, m_i, is influenced by the gravitational force exerted by m_q as well as other perturbing bodies, m_j, included in the model. It is assumed in this model that each body is a centrobaric point mass and that the particle of interest possesses an infinitesimally small mass relative to other included bodies. The system of equations that results from this formulation governs the path of the particle of interest,

$$\ddot{\boldsymbol{p}}_{qi} = -G\frac{m_i + m_q}{p_{qi}^3}\boldsymbol{p}_{qi} + G\sum_{\substack{j=1 \\ j\neq i,q}} m_j\left(\frac{\boldsymbol{p}_{ij}}{p_{ij}^3} - \frac{\boldsymbol{p}_{qj}}{p_{qj}^3}\right) \tag{5}$$

where G is the universal gravitational constant, $\boldsymbol{p}_{qi}$ is the position vector from the central body to the particle of interest, and p_{qi} is the norm of this vector. Similarly, $\boldsymbol{p}_{ij}$ and $\boldsymbol{p}_{qj}$ are position vectors to the perturbing bodies from the particle of interest and the central body, respectively. The locations of the perturbing bodies at each instant of time in this model are obtained from the Jet Propulsion Laboratory's Navigation and Ancillary Information Facility (NAIF) SPICE ephemeris data. Because this application focuses on trajectories in the Earth-Moon system, near to the Moon, the Moon is employed as the central body, m_q, while the Earth, Sun, and Jupiter are incorporated as significant perturbing bodies. Finally, the particle of interest is assumed to be a spacecraft whose initial epoch is defined at midnight on January 25^{th}, 2025.

B. Direct Transcription Framework

Typically, the goal in low-thrust trajectory design is an optimal path. Given an adequate initial guess, the desirable trajectory is one that satisfies the mission constraints while minimizing a given objective, often the propellant consumption or the time of flight. The optimization problem is continuous, that is, at each instant along the path a thrust direction and magnitude must be identified to optimize the objective. A wide array of strategies are available to solve this type of problem and one particularly powerful approach is direct transcription. A direct transcription technique utilizes a collocation scheme to discretize the continuous optimal control problem such that it can be solved via a direct optimization method [18, 19]. Collocation is a method of numerical integration that is employed within this context to integrate and update the initial guess for a low-thrust trajectory. This technique offers an alternative to the familiar shooting approach for trajectory corrections that demonstrates greater robustness, i.e., when provided a very poor initial guess collocation algorithms may converge to some solution when shooting schemes struggle. Thus, by coupling collocation with a direct optimization method, direct transcription delivers a robust approach for computing optimal low-thrust trajectories that is also amenable to the straightforward addition of boundary and path constraints.

A number of authors have demonstrated the application of direct transcription techniques to the problem of low-thrust trajectory design, particularly when lacking information for the construction of an initial guess. Ozimek, Grebow, and Howell apply direct transcription techniques to compute low-thrust enabled periodic orbits that supply communications coverage for the lunar south pole [20]. These authors employ a stack of nodes in the desired region of configuration space as an initial guess for a low-thrust trajectory; furthermore, the geometry of the resulting trajectory is bounded by enforcing path constraints. Likewise, Herman [9], as well as Parrish et al. [10], assemble stacks of ballistic trajectory arcs along the originating and destination orbits to generate initial guesses for low-thrust transfers in the Earth-Moon CR3BP. These straightforward strategies for initial guess construction are extended in this investigation to leverage chains of natural dynamical structures that serve as an initial guess for low-thrust transfer trajectories. The robust nature of collocation enables correction of a coarse initial guess into a continuous low-thrust trajectory. However, several

techniques are added to the standard collocation formulation to ensure convergence and to deliver practical low-thrust solutions.

The direct transcription formulation implemented in this analysis is described in detail in a previous investigation by Pritchett, Howell, and Grebow [12] where the resulting algorithm is denoted COLT (Collocation with Optimization for Low-Thrust). A major component of the COLT algorithm is the collocation scheme it employs; in this case, the collocation strategy is based on the framework developed by Grebow and Pavlak [21] and utilizes 7^{th} degree polynomials with Legendre-Gauss node spacing. Furthermore, the control with explicit propagation (CEP) mesh refinement strategy detailed by Grebow and Pavlak is employed to ensure that the collocation results are sufficiently accurate. In addition, problem specific constraints are enforced, as well as the standard collocation constraints, to assure that the collocation approach generates practical low-thrust trajectories. One of these constraints fixes the position and velocity components of the initial and final patch points along the trajectory to specific states, while another enforces a minimum altitude relative to one or both of the primaries. Constraints that force the thrust vector to be defined by a unit magnitude direction vector and possess a total magnitude below T_{max} are also enforced. Altogether, this framework ensures the collocation scheme utilized by COLT is able to converge to practical low-thrust trajectories.

The other fundamental part of the implementation of the COLT algorithm is its optimization framework. In this investigation, the third-party optimizer SNOPT (Sparse Nonlinear OPTimizer) is coupled with the collocation scheme to compute optimal trajectories [22, 23]. This optimizer uses a Sequential Quadratic Programming method and is well-suited for the sparse large-scale problems generated by collocation techniques. Several other strategies are implemented along with the selected optimizer to facilitate the optimization process. First, bounds are set for each design variable that restrict the range for the available values. The inclusion of such bounds limits the scope of the optimization problem and generally aids convergence. Furthermore, variable or constraint scaling may be applied to produce a better conditioned optimization problem and, thereby, improve accuracy and reduce run-time. These additional strategies, as well as careful selection of optimizer settings, lead to superior optimization results. In sum, COLT pairs a robust collocation scheme with a powerful optimization framework to generate optimal low-thrust trajectories.

C. Multiple Shooting Framework

In contrast with direct transcription, a multiple shooting framework need not include an optimization algorithm to deliver a solution given a discretized initial guess. Thus, implementation of a multiple shooting method is straightforward and easily applicable to impulsive transfer design. As discussed in depth by Zimovan [24], a multiple shooting process entails solving several two-point boundary value problems simultaneously to meet a selected set of design constraints. To implement this scheme, an initial guess for a trajectory is formulated using n patch points, or nodes, that separate $(n-1)$ segments. Note, this is the same discretization employed to define segments in the direct transcription formulation. State continuity (position, velocity, and time as appropriate) is enforced at each patch point along with any other user-defined constraints, e.g., altitude or flight path angle. However, for impulsive maneuvers, velocity continuity is omitted from the formulation. Following the formulation of the two point boundary value problem, a linear differential corrections process is used to converge upon a solution. This process uses elements of a state transition matrix and other partial derivatives to relate downstream variational state elements to variational elements corresponding to control variables at the patch points located upstream. A detailed formulation and examples of this strategy are availabe in Reference [24].

As part of this investigation, a multiple shooting scheme is implemented to compute impulsive transfers based on initial guesses from low-thrust trajectories that are constructed by applying direct transcription to discontinuous orbit chains. When low-thrust trajectories are employed as an initial guess, patch points are placed along the trajectory at the same locations used in the discretized direct transcription solution; continuity is then enforced at each of these nodes. However, impulsive maneuvers are allowed at patch points that correspond to the beginning of thrusting segments along the low-thrust trajectory. A variable-time multiple shooting strategy is employed, thus, the time between patch points is allowed to shift. Therefore, the total transfer time is likely to vary from the transfer time required for the corresponding low-thrust solution. This framework is employed to transition low-thrust transfers to impulsive trajectories in the CR3BP. Furthermore, this capability is advantageous because employing a low-thrust solution as an initial guess for an impulsive transfer may offer novel transfer characteristics that would not be available from techniques conventionally employed to construct impulsive transfers. Therefore, approaches used to design transfers in a low-thrust regime, for example, an orbit chaining method, may be exploited to aid the construction of impulsive transfers as well.

D. Orbit Chain Construction

Presently, initial guess construction is one of the most challenging aspects of transfer design for both low-thrust as well as impulsive spacecraft path planning in a complex regime. Differential corrections schemes typically require an initial guess for the six-dimensional state time history along a transfer; this initial guess is then refined into a continuous trajectory that meets prescribed constraints. The characteristics of an initial guess significantly influence the converged solution, thus, a well constructed initial guess is critical to producing a desired outcome for various control methodologies, e.g., low-thrust or impulsive capabilities. The solution space available for a transfer is typically comprised of one or more feasible solution types–each characterized by a particular basin of convergence. When the input to a corrections algorithm, the initial guess, lies within the desired basin of convergence, the corrections process yields a solution that possesses certain characteristics common to that solution basin. Given the infinite number of potential initial guesses available for a transfer design, as well as the sensitivity of the final solution to the initial guess, it is advantageous to develop a systematic approach for constructing initial guesses and exploring different basins of convergence. However, creation of such an approach is challenging, especially with the option of incorporating low-thrust propulsion. Thus, additional techniques that direct the solution toward a set of desired characteristics are sought.

A common approach for initial guess construction is assembling known dynamical structures into a "chain" with state discontinuities to be corrected with the addition of impulsive or low-thrust engine burns, as illustrated in Figure 1. Within the context of the CR3BP, the invariant manifolds of unstable periodic orbits are frequently introduced as intermediate dynamical structures available for construction of the initial guess "chain", particularly for transfers between two such orbits. Numerous authors have demonstrated that this approach provides low-energy connections between orbits. For example, Barden, Howell, and Lo [25, 26] employ invariant manifolds to facilitate transfer design within the Earth-Moon CR3BP while Koon et al. [27] and Gomez et al. [28] offer strategies that employ invariant manifolds to link multiple periodic orbits, thereby forming complex transfer itineraries that span large regions in the CR3BP phase space. However, beyond the inherent manifold structures associated with the originating and destination periodic orbits, resonant orbits and their manifolds also supply natural dynamical structures that are advantageous for transfer design in the CR3BP. For example, Vaquero and Howell leverage the manifolds of resonant orbits to develop tours between several libration point orbits [29]. These examples from prior applications illustrate just two of the many options for intermediate arcs in the formation of initial guesses to support transfer design.

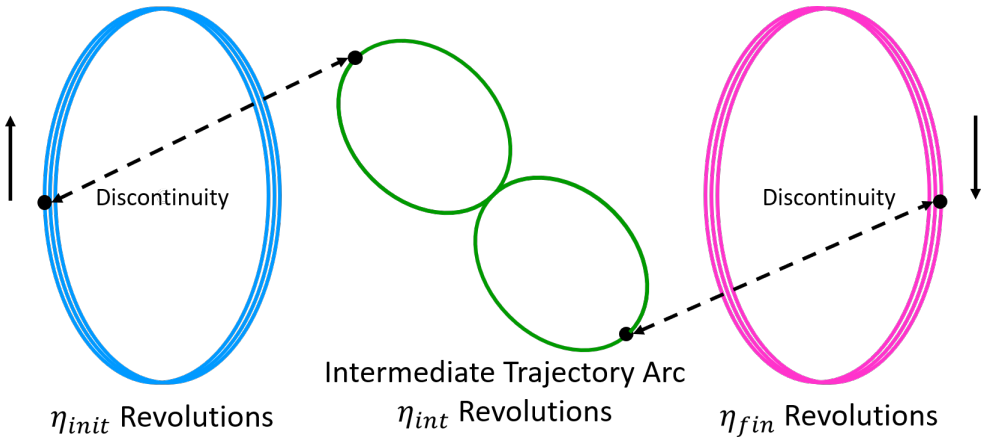

Fig. 1 Illustration of the orbit chaining technique. The diagram depicts a three-link orbit chain comprised of three different periodic orbits where each link in the chain has η_k stacked revolutions

While trajectory design strategies that incorporate invariant manifolds often deliver low-energy transfers, the process of generating many manifolds from orbits of interest, then searching for low-cost intersections is frequently tedious and computationally expensive. Moreover, some orbits of interest in the CR3BP are stable or nearly-stable and, thus, invariant manifolds do not directly assist with transfer design to and from these orbits. To address such limitations, alternative techniques for transfer construction are formulated. Restrepo and Russell [30] demonstrate a method of patched periodic orbits (PPO) to develop low-energy transfers by linking periodic orbits selected from a pre-computed catalog with very low Δv maneuvers; Haapala and Howell apply a similar technique using a catalog of periodic orbits

in the CR3BP [31]. Likewise, Pritchett, Howell, and Grebow [12] utilize an orbit chaining method to develop initial solutions for low-thrust transfers that are converged using a direct transcription scheme; a similar strategy is the basis of this investigation. The orbit chaining approach allows transfers with a wide variety of itineraries and characteristics to be constructed simply by assembling different combinations of known dynamical structures.

To construct an orbit chain, segments from one or more dynamical structures are assembled into a sequence that facilitates a transfer between regions in the CR3BP phase space. Each segment employed in an orbit chain is comprised of two or more nodes that include position, velocity, and control information. The initial and final links in an orbit chain are determined by the departure and arrival orbits for the desired transfer, thus, the first step in the construction of a chain is the selection of these orbits. The simplest orbit chains are comprised solely of segments that lie on the departure and arrival orbits. Multiple revolutions along these or other orbits in a chain are included by "stacking" segments of the same type. For example, three revolutions along an NRHO can be included in an orbit chain by discretizing one revolution along the orbit into segments, duplicating these segments three times, and concatenating the states associated with these segments into a single vector. For orbit chains with intermediate links between the departure and arrival orbits, the second step in the construction process is the selection of useful natural dynamical structures. Phase space geometry is employed to select the families of natural dynamical structures that are considered for intermediate links in an orbit chain. Hence, the first families examined are those with geometries that intersect, in position or velocity space, neighboring links in an orbit chain. Within a family of trajectory arcs, Jacobi constant value is the primary metric currently used for the selection of favorable candidates for intermediate links. The initial and final Jacobi constant values representing the path of the third body across a transfer arc are determined by the departure and arrival orbits defined in terms of Jacobi constant values, J_0 and J_f, respectively. The dynamics in the CR3BP dictate that the Jacobi constant value corresponding to the third body path must pass through all values of the Jacobi constant between J_0 and J_f, thus, intermediate arcs with Jacobi values between those of the originating and destination orbits serve as viable candidates. Plots such as those in Figure 2(a) assist with the selection of the intermediate arcs by displaying the members of a family within a range that possesses Jacobi constant values between those of the originating and destination orbits that define the transfer. In this example, a member of the L_4 short period orbit family is selected to facilitate a transfer from a DRO to an L_3 Lyapunov orbit. Position and velocity differences between the final and initial points on the neighboring links in an orbit chain may also be employed to select intermediate arcs within a family. For example, Figure 2(b) illustrates an orbit chain constructed for a transfer from a 9:2 synodic resonance NRHO to a member of the L_2 southern halo family with $A_z = 13,977.16\ km$. This chain does not solely employ intermediate links with Jacobi constant values between J_0 and J_f. The distance between neighboring links is also considered when constructing this orbit chain which consists of multiple members of the L_2 Southern halo family. In summary, selection of the trajectory arcs that represent each link along an orbit chain, as well as the number of revolutions along an intermediate orbit for stacking in the creation of each link, are significant first steps in the orbit chain construction process.

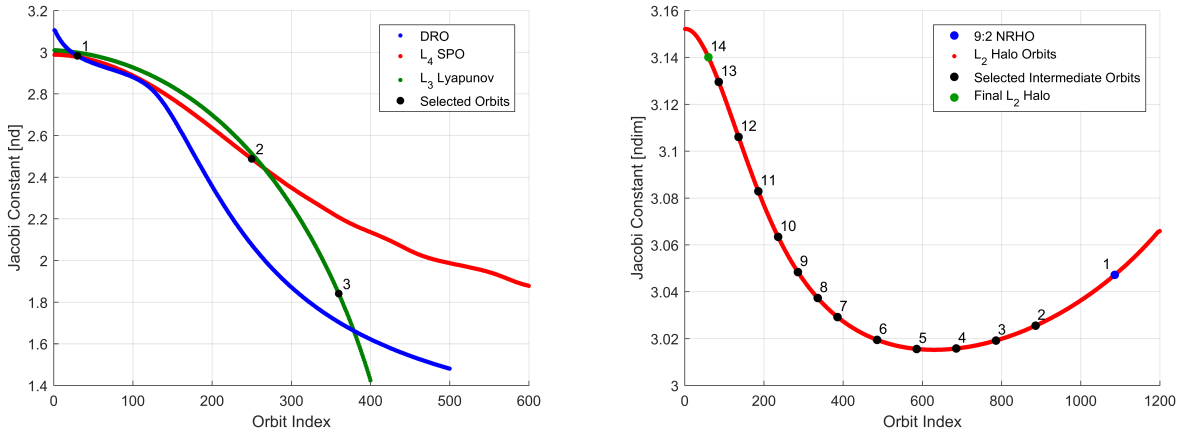

(a) for DRO to L_3 Lyapunov Transfer

(b) for 9:2 NRHO to L_2 Southern Halo Transfer

Fig. 2 Plots of Jacobi constant value as a function of orbit index used to construct orbit chains that serve as initial guesses for two different transfers.

Once the links that comprise an orbit chain are selected, the next step is to concatenate nodes from segments along each link into a single vector of state and control values to be passed to the direct transcription algorithm. Note, the dynamical structures used for each link offer initial values for the position and velocity states along the transfer, but they do not dictate the control values. Typically, in this analysis, the initial thrust vector magnitude is set equal to 0 N, while the initial thrust direction is aligned with the direction of the velocity vector at each node. The nodes at the intersection of two orbit chain segments almost always include some discontinuities in position, velocity, or the control values, and these discrepancies are corrected by the direct transcription process. The simple orbit chain construction procedure is straightforward for incorporating any number of links into the orbit chain, and additional links are added if the discontinuities between segments are large.

After an orbit chain is assembled, it is passed to a direct transcription procedure that corrects the discontinuous initial guess into a continuous path. The settings and the number of simulation runs required of the direct transcription algorithm are determined by the characteristics of the desired trajectory. The direct transcription scheme employed in this investigation is implemented such that the converged result always includes thrust and coast segments, rather than impulsive burns. However, an "impulsive-like" transfer can be generated from an orbit chain by running COLT with a high value of T_{max}. This setting often leads to low-thrust transfers with few thrust segments that leverage large thrust magnitudes. This type of low-thrust transfer is then simpler to transition into an impulsive trajectory using the process of converting thrust segments to impulsive maneuvers. Alternatively, in scenarios where a low-thrust trajectory is sought, the direct transcription scheme may struggle to converge for the specified value of T_{max}. It is sometimes advantageous to first converge a trajectory using a higher value of T_{max}, then employ continuation to reduce the value of T_{max} to the desired level. Together, these procedures successfully generate low-thrust or impulsive transfers despite the coarse initial paths supplied by the orbit chains.

IV. Orbit Chaining Examples

Sample applications of an orbit chaining approach are offered to demonstrate the suitability of this technique for a wide array of problems. Different three-link orbit chains are assembled to demonstrate that, for the same departure and arrival orbits, the type of intermediate trajectory arc included in a chain influences the characteristics of the final low-thrust solution. Additionally, orbit chains with a greater number of intermediate arcs are assembled to exhibit the versatility of the orbit chain approach. Finally, the type or number of intermediate links included in any of the sample orbit chains may be modified to generate low-thrust transfers that meet different problem specific constraints.

A. Three-Link Orbit Chains

An infinite number of trajectory arcs are available for orbit chains. However, when only one type of intermediate arc is incorporated to link the departure and arrival orbits, the impact of the intermediate arc selection on the characteristics of the final solution is plainly evident. Three-part orbit chains include revolutions along the departure and arrival orbits as well as all or part of an intermediate arc. For this type of orbit chain, two examples, appear in Figure 3, where two different three-link orbit chains are employed to design a transfer from a DRO with a Jacobi constant value $J = 2.9822$ and a perilune $r_p = 41,000\ km$ to an L_3 Lyapunov orbit with $J = 1.8402$. In Figure 3(a), a segment from a member of the 2:3 resonant orbit family with $J = 2.3540$ is employed whereas, in Figure 3(b), a full revolution along a L_4 short period orbit, $J = 2.4879$, is selected as an intermediate arc. Note, as discussed previously, the Jacobi constant values for both intermediate arcs fall between the Jacobi constant values associated with the departure and arrival orbits. In the sample transfers in Figure 3, for both choices of intermediate arcs, large discontinuities exist at the intersections with the intermediate arc. However, despite these discontinuities, the initial guesses constructed from both types of orbit chain are converged using direct transcription to yield low-thrust transfers that are local optima. The optimal low-thrust transfers that result from the two different initial guesses are displayed in Figures 3(c) and 3(d). These trajectories clearly reflect the geometry of their respective initial guesses. Information on the final mass, time of flight, and equivalent Δv that characterize these transfers, and others in this section, are included in Table 1. The results from this initial three-link orbit chain suggest a "recipe" for the initial guess composition with the orbit chaining method, whereby different combinations of intermediate arcs yield optimal transfer solutions with particular types of characteristics. This strategy for the initial guess construction is tested with several more three-link orbit chains.

Transfers constructed in the vicinity of the smaller primary body offer another scenario where the utility of an informed approach to assembling the orbit chains is evident. In this case, a transfer from an L_2 Lyapunov orbit with a Jacobi constant value $J = 2.9830$ and a perilune distance $r_p = 10,316.68\ km$ to a DRO orbit with $J = 2.8648$ and $r_p = 111,566.45\ km$ is examined. In Figure 4(a), a segment of a period three DRO with $J = 2.8735$ is employed as

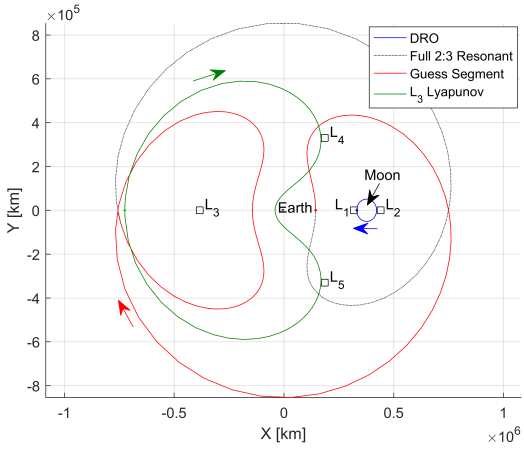

(a) Initial guess with 2:3 resonant orbit intermediate arc

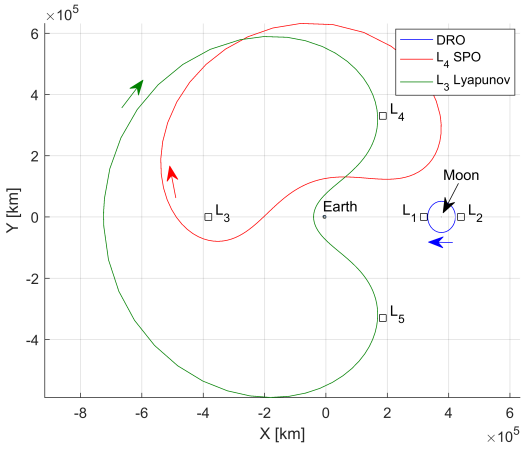

(b) Initial guess with L_4 short period orbit intermediate arc

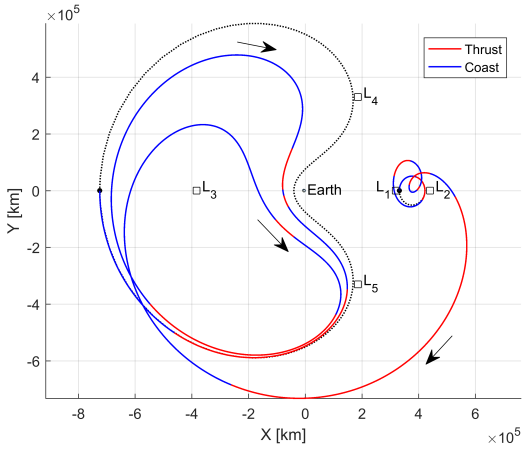

(c) Optimal low-thrust transfer from initial guess in (a)

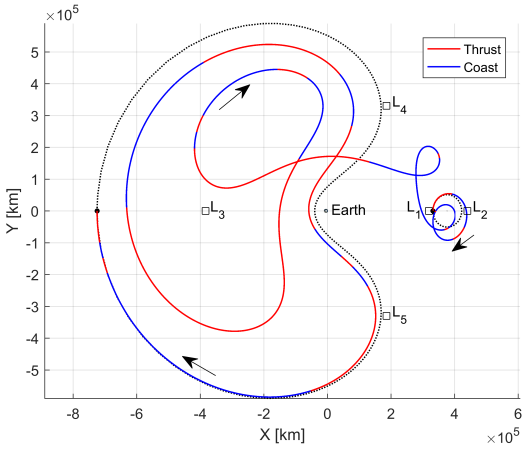

(d) Optimal low-thrust transfer from initial guess in (b)

Fig. 3 Initial guesses and optimal low-thrust solutions for three-link orbit chains that utilize two different types of intermediate arcs to construct a transfer from a specified DRO to a L_3 Lyapunov orbit. Transfers are for a spacecraft with $m_0 = 1000\ kg$, $T_{max} = 200\ mN$, and $I_{sp} = 2000\ sec$.

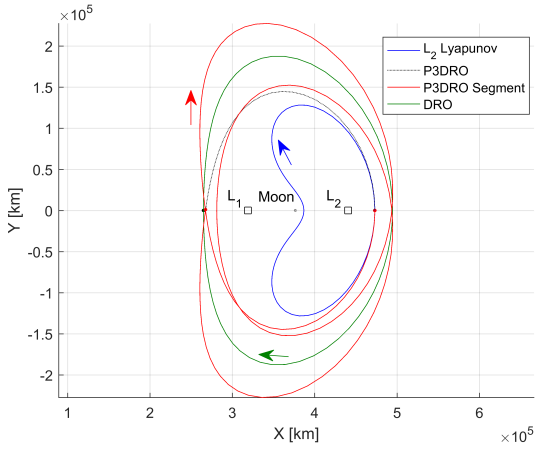

(a) Initial guess with period three DRO intermediate arc

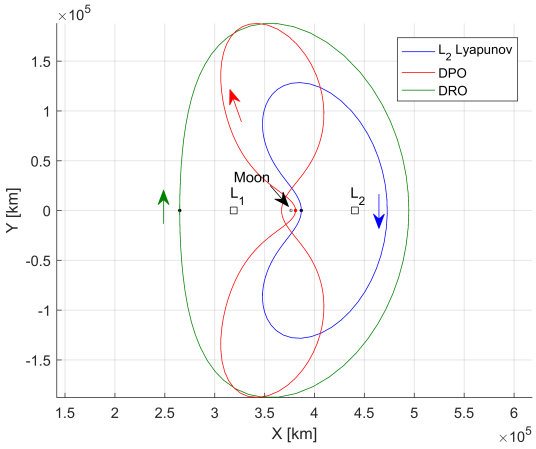

(b) Initial guess with distant prograde orbit intermediate arc

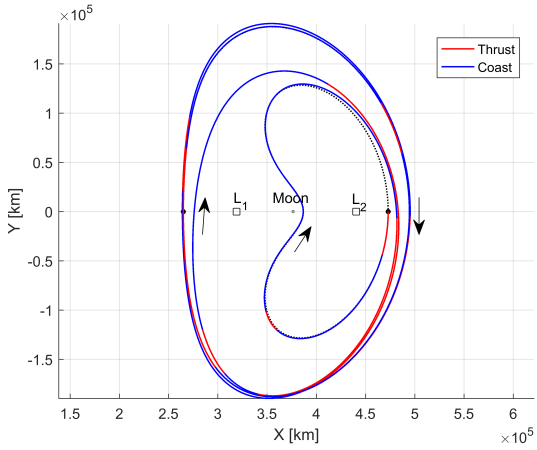

(c) Optimal low-thrust transfer from initial guess in (a)

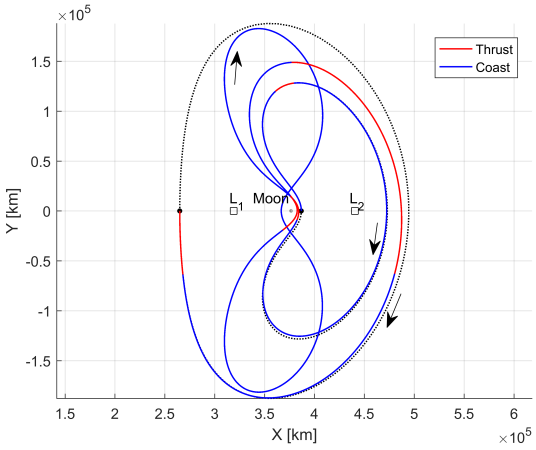

(d) Optimal low-thrust transfer from initial guess in (b)

Fig. 4 Initial guesses and optimal low-thrust solutions for three-link orbit chains that utilize two different types of intermediate arcs to construct a transfer from an L_2 Lyapunov orbit to a DRO. Transfers are for a spacecraft with $m_0 = 1000\ kg$, $T_{max} = 200\ mN$, and $I_{sp} = 2000\ sec$.

an intermediate arc in an orbit chain. Alternatively, in Figure 4(b), a full revolution along a distant prograde orbit (DPO), $J = 2.9732$, is selected as an intermediate arc. The locally optimal low-thrust transfers that result from both combinations of three-link orbit chains appear in Figures 4(c) and 4(d), respectively. Exploiting a P3DRO in an orbit chain generates a low-thrust transfer with a 94-day time of flight, and $\Delta v = 156.23\ m/s$. In contrast, the orbit chain that includes a DPO leads to a transfer that utilizes a close approach to the Moon to reach the destination orbit with a shorter time of flight and only a marginally higher Δv. This example demonstrates the effectiveness of the intermediate arcs employed in an orbit chain in producing the desired characteristics for the resulting low-thrust transfer.

Chains are also leveraged to accommodate large plane changes. The final three-link orbit chain is examined to produce a transfer from a 9:2 synodic resonant NRHO ($J = 3.0471$) with a perilune radius $r_p = 3,125.51\ km$ to a DRO ($J = 2.9328$) with a perilune distance of $r_p = 70,000.00\ km$. Transfer design between these two orbits is challenging due to the large plane change that is required. Furthermore, the increased number of natural dynamical structures available for constructing a transfer offers an overwhelming number of potential paths. A segment from a 2:3 resonant

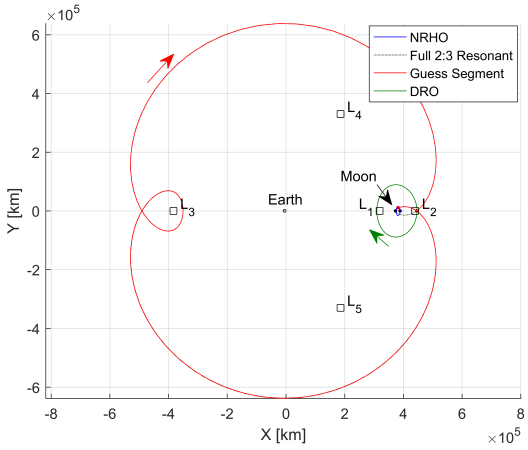

(a) Initial guess with 2:3 resonant intermediate arc

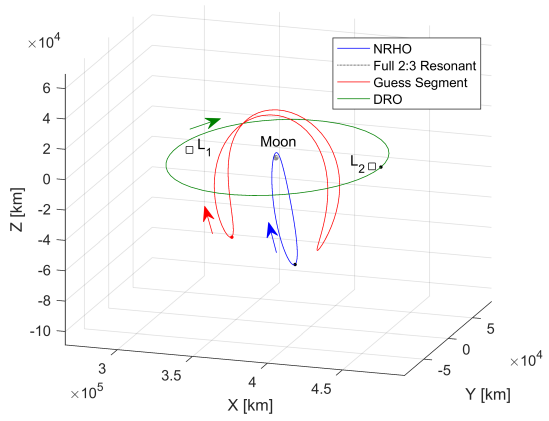

(b) Initial guess with a southern butterfly orbit intermediate arc

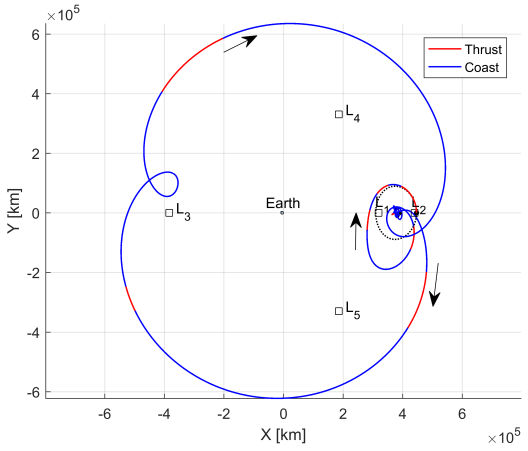

(c) Optimal low-thrust transfer from initial guess in (a)

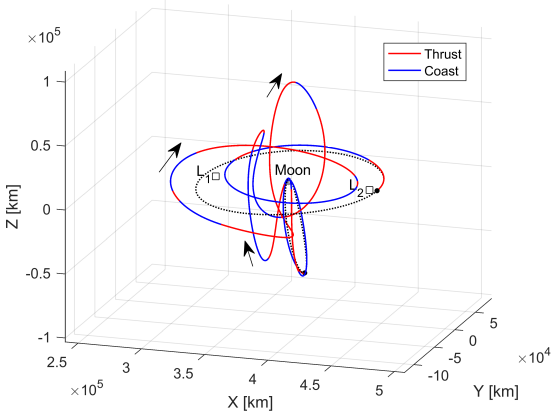

(d) Optimal low-thrust transfer from initial guess in (b)

Fig. 5 Initial guesses and optimal low-thrust solutions for three-link orbit chains that utilize two different types of intermediate arcs to construct a transfer from an NRHO to a DRO. Transfers are for a spacecraft with $m_0 = 1000\ kg$, $T_{max} = 200\ mN$, and $I_{sp} = 2000\ sec$.

orbit, displayed in Figure 5(a), with $J = 2.9606$, is one of the intermediate arcs selected for constructing a transfer between the NRHO and DRO. This orbit covers a large region in configuration space and remains far from either primary during the majority of its transit. Thus, when included as an intermediate arc in an orbit chain, this geometry is

transformed to allow the required plane change to occur gradually and far from either of the primaries. These features are beneficial for reducing the Δv necessary to achieve the transfer, however, such a geometry also significantly increases the time of flight. Alternatively, an intermediate arc with a significant out-of-plane component reduces the required transfer time at the cost of increased Δv. In this example, a southern butterfly orbit, plotted in Figure 5(b), with $J = 3.0830$, is selected. Note that the Jacobi constant value for this intermediate arc is beyond the range of values defined by J_0 and J_f. The butterfly orbit is selected, not based on its Jacobi constant value, but because the difference in velocity magnitude between the final node along the NRHO orbit and the initial node along the butterfly orbit is smaller than any other member of the southern butterfly family. This criteria proved to be a better basis for selecting an intermediate arc if a quick delivery is preferred in this scenario. The low-thrust transfers generated from both of these sample orbit chain configurations are displayed in Figures 5(c) and 5(d) and, not surprisingly, it is evident that these transfers preserve some characteristics of the orbit chains used to construct them. The transfer that results when a 2:3 resonant orbit segment is employed as an intermediate arc possesses a longer time of flight than the transfer that uses a butterfly orbit, however, the latter transfer requires approximately 222 m/s more Δv than the former. The results in Figures 3 through 5 demonstrate that some orbit chains are better suited for constructing low-thrust transfers with specific characteristics than others. For example, if the geometry of the intermediate arc in a three-link orbit chain is ill-suited for facilitating a transfer between the departure and arrival orbits, then the result significantly distorts the geometry of the intermediate arc to achieve a mass optimal transfer. The transfers in Figures 3(d) and 5(d) are representative of this effect because they least resemble the geometry of the orbit chain used to generate them. This type of result indicates that a different intermediate arc is likely a better option to construct the desired low-thrust transfer. However, while these intermediate arcs struggle with mass optimal transfers, they may be more favorable for designing time optimal transfers. The six different low-thrust transfers computed using three-link orbit chains are summarized in Table 2. While three-link orbit chains offer simple demonstrations of the impact of different intermediate arcs on the final geometry, this technique for initial guess construction is more often effective when multiple intermediate arcs are incorporated.

Table 2 Low-thrust transfers constructed from three-link orbit chains and examined for a spacecraft with $m_0 = 1000\ kg$, $T_{max} = 200\ mN$, and $I_{sp} = 2000\ sec$.

Transfer Type	$TOF\ (days)$	$\Delta m\ (kg)$	m_f/m_0	$\Delta v\ (m/s)$
DRO → L_4 SPO → L_3 Lyapunov	70.0966	32.6313	0.9674	650.6823
DRO → 2:3 Resonant → L_3 Lyapunov	91.5769	30.2737	0.9697	602.9403
L_2 Lyapunov → P3DRO → DRO	94.1852	7.9340	0.9921	156.2332
L_2 Lyapunov → DPO → DRO	74.7037	5.5744	0.9944	109.6388
NRHO → 2:3 Resonant → DRO	121.3350	12.9961	0.9870	256.5670
NRHO → Butterfly → DRO	57.6456	24.1019	0.9759	478.5069

B. Multi-Link Orbit Chains

An infinite number of natural dynamical arcs can be linked to construct an initial guess in an orbit chaining approach. Powered arcs may also be available but are not included in this analysis. Often, including more than one intermediate arc between the specified departure and arrival orbits in an orbit chain reduces the state discontinuities between links in the chain, improving the convergence of the direct transcription algorithm. In this investigation, several types of multi-link orbit chains are constructed to facilitate transfers between periodic orbits in the Earth-Moon system, particularly when the originating and destination orbits are stable or nearly so. The first multi-link chain is an initial guess for a transfer from an L_1 Lyapunov orbit ($J = 3.0012$) to a large DRO ($J = 2.2059$) with radius of perilune $r_p = 302,105.58\ km$. Figure 6(a) displays that several DROs with higher values of J and lower r_p distances with respect to the Moon are included in the orbit chain to offer intermediate steps between the departure and arrival orbits. The more intermediate arcs that are included in the initial guess, the smaller each discontinuity, however, the additional arcs also increase the time of flight along the resulting path. Including 6 intermediate DROs in the orbit chain produces the optimal low-thrust transfer plotted in Figure 6(b). While the geometry of the optimal transfer is significantly shifted from that of the initial guess, it does leverage a spiraling motion to reach the final orbit that is similar to the structure of the initial guess. Moreover, the number of revolutions during the spiraling process that are leveraged to reach the destination orbit is influenced by the number of intermediate arcs that are included in the initial guess. The final mass, Δv, and time of flight for this transfer, as well as all others included in this section are summarized in Table 3. This transfer demonstrates that including multiple members of a periodic orbit family as links in an orbit chain is useful to develop transfers that

gradually transition along members of an orbit family to reach the desired final orbit; the strategy is easily applied to other families.

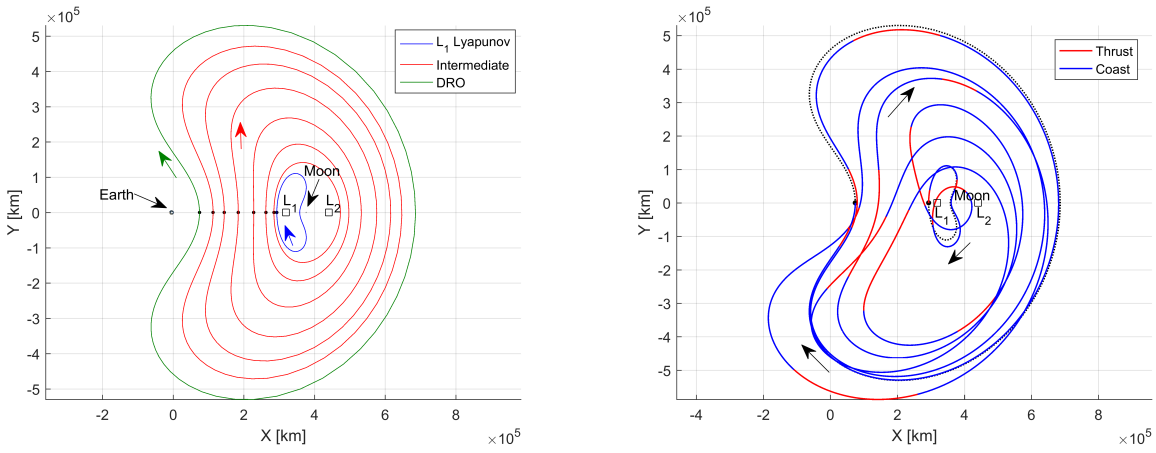

(a) Initial Guess

(b) Optimal Low-Thrust Transfer

Fig. 6 Initial guess and optimal low-thrust solution for a multi-link orbit chain that utilizes multiple members of the DRO family to construct a transfer from an L_1 Lyapunov orbit to a large DRO. Transfer employs a spacecraft with $m_0 = 1000\ kg$, $T_{max} = 200\ mN$, and $I_{sp} = 2000\ sec$.

In the CR3BP, many periodic orbit families evolve via bifurcations, e.g., the L_2 halo orbit family bifurcates from the L_2 Lyapunov orbit family. Knowledge of these bifurcations is also exploited to design transfers between members of periodic orbit families. Such a sample transfer is accomplished from an L_2 Lyapunov orbit to an L_2 vertical orbit via the family of L_2 axial orbits. The L_2 axial family of orbits bifurcates from the L_2 Lyapunov orbit family; furthermore, the L_2 vertical orbit family bifurcates from this axial orbit family. Thus, a transfer from an L_2 Lyapunov orbit to an L_2 vertical orbit is designed by constructing an orbit chain that utilizes multiple members of the L_2 axial orbit family with Jacobi constant values between those of the departure and arrival orbits. This orbit chain appears in Figure 7(a) and includes six members of the L_2 axial orbit family. This orbit chain generates the optimal low-thrust transfer in Figure 7(b) which retains largely the same geometry as the initial guess with coast arcs along segments that resemble members of the axial orbit family and thrust arcs mostly occurring when the transfer crosses the X-Y plane.

Low-thrust transfers from low lunar altitude NRHOs to members of the halo orbit family nearer the Earth-Moon L_2 libration point are currently of great interest in the astrodynamics community. The NRHOs are strong candidates for long term placement of a space station near the Moon, however, spacecraft departing such a station with the intent of departing the Earth-Moon system may seek to leverage lower energy halo orbits that are nearer the L_2 Lagrange point. Therefore, transfers between these two types of halo orbits are desired. In this investigation, a transfer from a 9:2 synodic resonance NRHO with a lunar pass at a distance of $r_p = 3,125.51\ km$ to a L_2 halo orbit ($J = 3.1401$) with $A_Z = 13,977.16\ km$ is examined. In contrast to the previous transfers, this scenario employs a spacecraft with parameters that approximate those of the current Deep Space Gateway concept, i.e., $m_0 = 40\ mT$, $T_{max} = 1.2\ N$, and $I_{sp} = 2000\ sec$. These engine characteristics lead to the acceleration level in Table 1 for the large spacecraft model which is several orders of magnitude lower than the model employed for the previous transfer cases. To design this transfer, an orbit chain is constructed using the departure and arrival orbits as well as nine members of the L_2 southern halo orbit family; this chain is displayed in Figure 8(a). The optimal low-thrust transfer produced by this orbit chain is displayed in Figure 8(b) and it clearly exhibits a spiraling behavior that is influenced by the structure of the initial guess. However, rather than evenly spacing the spiraling along the L_2 southern halo family, the optimization process clusters loops along the optimal transfer into distinct groups. This result demonstrates that the orbit chaining technique is a suitable method for designing low-thrust transfers even for a low-thrust engine with quite low acceleration levels.

Finally, a different type of multi-link orbit chain is explored for the creation of a transfer for the large spacecraft model that originates from the vicinity of the Earth and delivers the spacecraft to an orbit about the Moon. This transfer is initially framed under the assumption that the spacecraft inserts onto the stable invariant manifold of a L_2 Lyapunov orbit following a trans-lunar injection (TLI) maneuver. Insertion onto this manifold occurs at its periapse with respect to

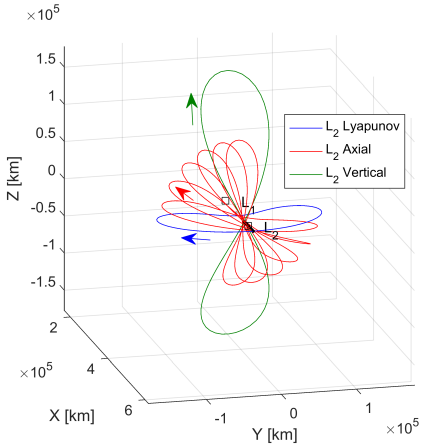

(a) Initial Guess

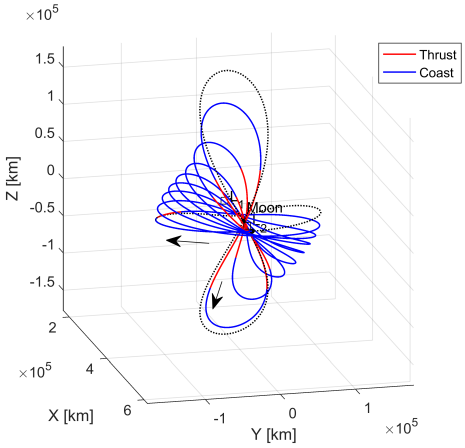

(b) Optimal Low-Thrust Transfer

Fig. 7 Initial guess and optimal low-thrust solution for a multi-link orbit chain that utilizes multiple members of the L_2 axial family to construct a transfer from a L_2 Lyapunov orbit to a large L_2 vertical orbit. Transfer is for a spacecraft with $m_0 = 1000\ kg$, $T_{max} = 200\ mN$, and $I_{sp} = 2000\ sec$.

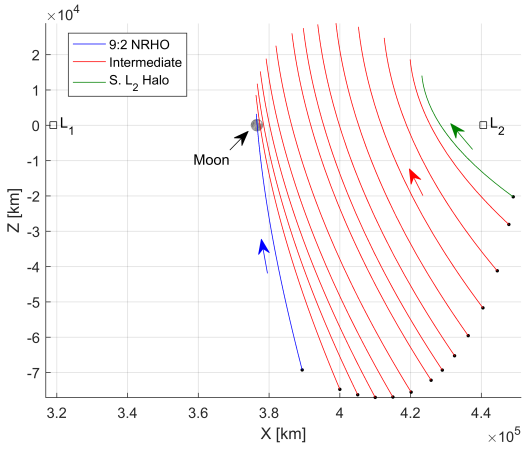

(a) Initial Guess

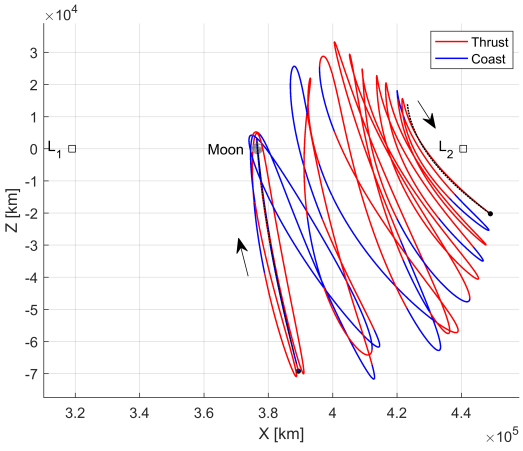

(b) Optimal Low-Thrust Transfer

Fig. 8 Initial guess and optimal low-thrust solution for a multi-link orbit chain that utilizes multiple members of the L_2 southern halo family to construct a transfer from a NRHO to a member of the L_2 southern halo family with $A_Z = 13,977.16\ km$. Transfer is for a spacecraft with $m_0 = 40\ mT$, $T_{max} = 1.2\ N$, and $I_{sp} = 2000\ sec$.

the Earth that occurs at a radius of $r_p = 55,291.65\ km$. The stable manifold of the L_2 Lyapunov orbit is the initial link in the orbit chain designed for this transfer while the final link is the destination L_2 southern halo orbit with $J = 3.1401$. The intermediate links along the chain include the L_2 Lyapunov orbit from which the stable manifold originates as well as several other members of the L_2 Lyapunov and L_2 southern halo orbit families. These orbits are assembled into the orbit chain displayed in Figure 9(a) that spans the Earth-Moon system. This orbit chain is easily converged to an optimal low-thrust transfer from the vicinity of the Earth to the final L_2 southern halo orbit. The path from the Earth to the lunar region largely follows that of the stable manifold employed as part of the initial guess. However, as the transfer evolves out of the X-Y plane and into the final halo orbit, the intermediate arcs included in the orbit chain are blended together to deliver a gradual transition into the destination orbit that appears to leverage some quasi-periodic structures near the L_2 Lagrange point. This transfer further demonstrates that the orbit chain approach can incorporate a large number of intermediate arcs including segments from invariant manifold structures. Note that future work includes the expansion of this orbit chain to incorporate the initial parking orbit.

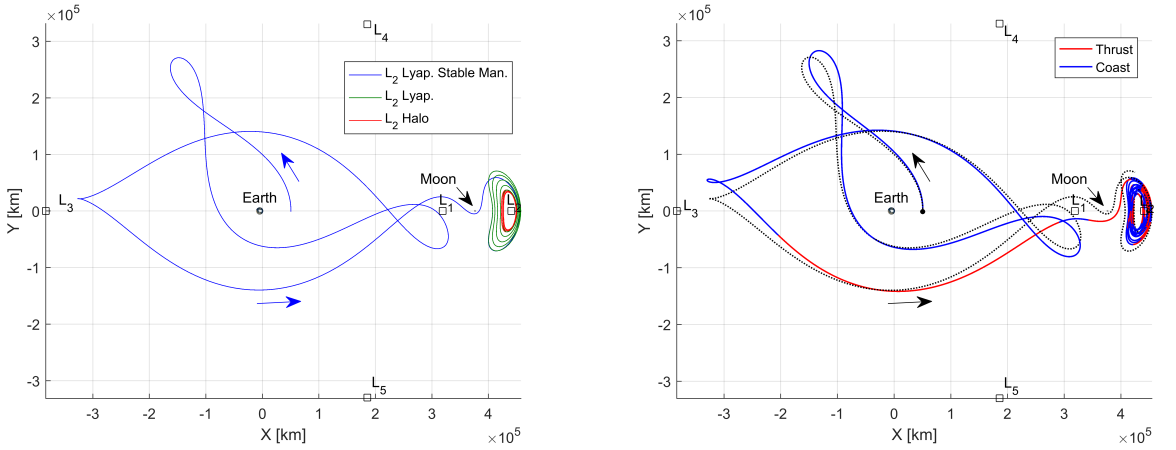

(a) Initial Guess

(b) Optimal Low-Thrust Transfer

Fig. 9 Initial guess as well as the optimal low-thrust solution for a multi-link orbit chain that utilizes multiple types of intermediate arcs including a segment of an invariant manifold to construct a transfer from a high-altitude Earth orbit to a L_2 southern halo orbit. Transfer is for a spacecraft with $m_0 = 40\ mT$, $T_{max} = 1.2\ N$, and $I_{sp} = 2000\ sec$.

Table 3 Low-thrust transfers constructed from multi-link orbit chains and examined for a spacecraft with $m_0 = 1000\ kg$, $T_{max} = 200\ mN$, and $I_{sp} = 2000\ sec$.

Transfer Type	$TOF\ (days)$	$\Delta m\ (kg)$	m_f/m_0	$\Delta v\ (m/s)$
L_1 Lyapunov $\rightarrow 6 \times$ DRO $\rightarrow$ DRO	187.9611	22.3211	0.9777	442.7496
L_2 Lyapunov $\rightarrow 6 \times L_2$ Axial $\rightarrow L_2$ Vertical	155.9287	14.5470	0.9855	287.4102
NRHO $\rightarrow 12 \times L_2$ Halo $\rightarrow L_2$ Halo	163.8251	592.3774	0.9826	292.6341
L_2 Lyapunov Manifold $\rightarrow 5 \times L_2$ Lyapunov $\rightarrow 5 \times L_2$ Halo	193.9883	344.3616	0.9914	169.5827

In all the previous examples, the number of intermediate arcs in each multi-link orbit chain is selected based on intuition and experience with bridging intermediate discontinuities in any initial guess to accomplish a successful transfer. However, in every case, similar transfers are available when greater or fewer numbers of intermediate arcs are incorporated. Consequently, the time of flight along each transfer can be adjusted either by changing the number of intermediate arcs, or via a continuation process. These modifications also influence the geometry, and possibly the Δv cost, by removing excess trajectory and thrust arcs. A more rigorous framework for the selection of appropriate intermediate arcs may improve the transfer efficiency.

V. Transition Between Low-Thrust and Impulsive Transfers

The orbit chain approach and the direct transcription algorithm employed in this investigation is not limited to generating low-thrust transfers. In an extension of this work, the COLT algorithm is applied to a subset of the orbit chains assembled previously, to compute low-thrust transfers that employ a high value of T_{max}. A process for transitioning these continuous thrust transfers into an impulsive regime is described and the resulting transfers are displayed. Furthermore, the applicability of the direct transcription scheme to the conversion of impulsive transfers into low-thrust trajectories is tested. Finally, several impulsive trajectories obtained by using a low-thrust path as an initial guess are transitioned into an ephemeris model for validation.

A. Low-Thrust to Impulsive Transfer Initial Guess

Beyond applications involving low-thrust options, cislunar transfers between stable and nearly stable orbits also aim to utilize impulsive spacecraft type engine models. Impulsive solutions, similar to trajectories computed in the low-thrust case, also depend upon an initial guess. The transitioning of optimal transfers constructed using low-thrust direct transcription methods into impulsive solutions offers an alternative strategy to deliver impulsive transfers. In this investigation, the transition of low-thrust solutions into the impulsive regime begins with the selection of nodes for the multiple shooting impulsive framework. The converged solution from a direct transcription process, such as those examples that appear in Figures 3 through 9, is comprised of patch points (discretized nodes along a trajectory) that are linked by either thrusting or coasting arcs. These patch points are directly input to the multiple shooting framework to formulate the discretized initial guess. Continuity is enforced across all patch points with the exception that velocity discontinuities, or Δv's, are allowed at the patch points that correspond to the first point along a thrusting segment in the low-thrust solution. The initial and final patch points are held fixed in position at the departure and arrival locations along the corresponding periodic orbits. In this formulation of an initial guess, there is precisely one impulsive maneuver corresponding to each thrusting segment in the optimal low-thrust solution, one impulsive maneuver to depart the initial periodic orbits, and one impulsive maneuver for capture into the final periodic orbit.

Some sample impulsive transfers demonstrate the process. The low-thrust transfer in Figure 10(a) – a transfer from an L_2 Lyapunov orbit to a vertical orbit – is converted to an impulsive solution. This low-thrust transfer is similar to the one displayed in Figure 7, but it employs a higher maximum thrust value, $T_{max} = 1\ N$, therefore the thrusting segments are shorter in duration. The converged impulsive solution that results from this initial guess is plotted in Figure 10(b). In total, the impulsive transfer uses 6 intermediate impulsive maneuvers in addition to the maneuvers to depart and arrive on the Lyapunov and vertical orbits, respectively. Note that there are six thrusting segments along the low-thrust solution; the red dots along the final impulsive trajectory in Figure 10(b) correspond to the maneuver locations and display a one-to-one correspondence to the thrust arcs in the low-thrust initial guess. The total maneuver cost for this transfer is 475.7 m/s and the time of flight is 151.86 days. A geometry similar to the low-thrust transfer is maintained within the impulsive regime. The details of this transfer appear in Table 4

The low-thrust transfer between halo orbits appears in Figure 8. Developing an initial guess from a similar low-thrust result that employs $T_{max} = 40\ N$, the impulsive transfer between an L_2 NRHO and halo orbit is plotted in Figure 11. Note that, as in the prior example, there is one impulsive burn for each of the thrusting arcs along the low-thrust trajectory used for an initial guess (as indicated by red dots in Figure 11) as well as impulsive burns to depart the NRHO and arrive on the final halo orbit. As noted in Table 4, this transfer requires 352 m/s over a time of flight equal to 91.53 days.

Additional examples of transfers constructed via low-thrust initial guesses that are derived from various orbit chains are plotted in Figure 12. Note that the initial periodic orbit, an L_2 Lyapunov orbit, and the final periodic orbit, a DRO, are the same in both Figures 12(a) and 12(b), however, the intermediate orbit in the original "chain" significantly influences the low-thrust, and, thereby, the impulsive solution geometry. This effect is also seen in the corresponding low-thrust solutions in Figure 4. The transfer in Figure 12(a), solved using a period-three DRO as an intermediate arc, possesses 7 total burns resulting in a total transfer cost of 146.3 m/s with a time of flight of 74.69 days. The initial maneuver to depart the Lyapunov orbit only requires about 10 cm/s. Alternatively, the transfer in Figure 12(b), in which a distant prograde orbit is present in the initial orbit chain, has a total cost of 128.5 m/s over 6 total maneuvers and requires a time of flight of 94.3 days as summarized in Table 4. The initial and final propulsive maneuvers in this particular case are on the order of 10 cm/s.

As a final example of the transition of low-thrust solutions into the impulsive regime, a transfer between an NRHO and a DRO, plotted in Figure 13, is derived from the optimal low-thrust solution in Figure 5. Specifically, the intermediate arc employed in this transfer is a 2:3 resonant orbit; characteristics of this initial guess remain evident in the result. This transfer requires 11 intermediate maneuvers – 5 in close proximity to the Moon – in addition to departure and arrival

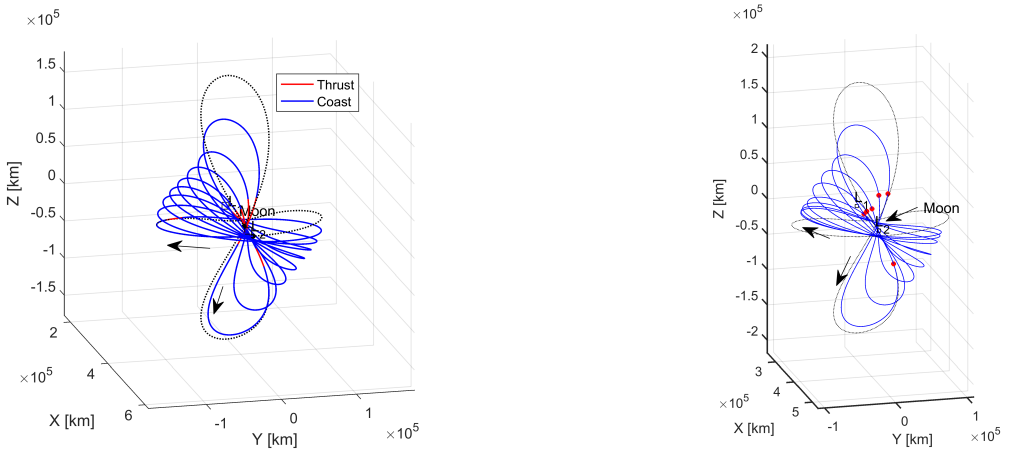

(a) Low-Thrust Transfer

(b) Impulsive Transfer

Fig. 10 Low-thrust and impulsive transfers from an L_2 Lyapunov orbit to a vertical orbit. The optimal low-thrust transfer in (a) uses the initial guess displayed in Figure 7(a) and a spacecraft with $m_0 = 1000\ kg$, $T_{max} = 1\ N$, and $I_{sp} = 2000$ sec. The impulsive transfer in (b) utilizes the optimal low-thrust transfer in (a) as an initial guess.

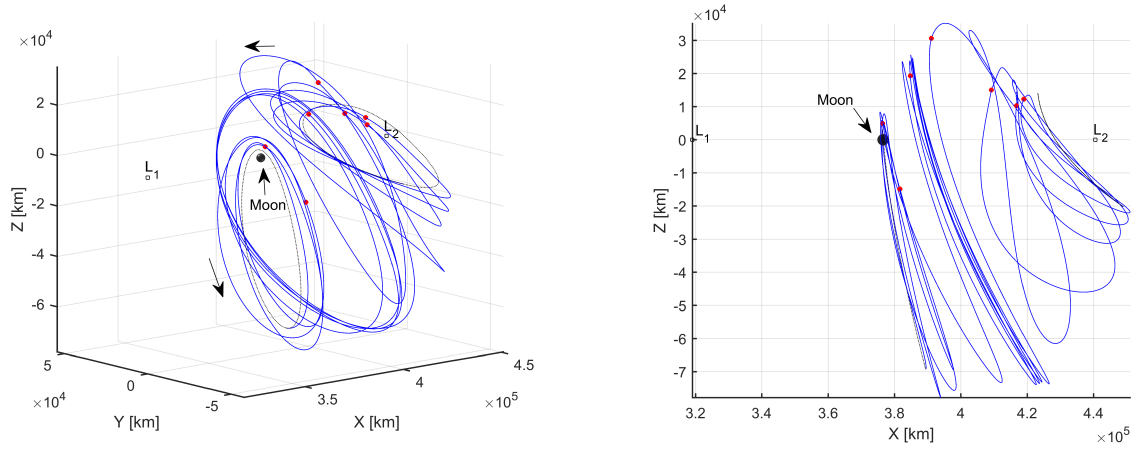

(a) Three-Dimensional View

(b) X-Z Plane View

Fig. 11 Low-thrust and impulsive transfers from a 9:2 NRHO to a L_2 halo orbit with $A_Z = 13,977.16\ km$ using an optimal low-thrust transfer solution similar to that in Figure 8, but with $T_{max} = 40\ N$, as the initial guess for the multiple shooting scheme.

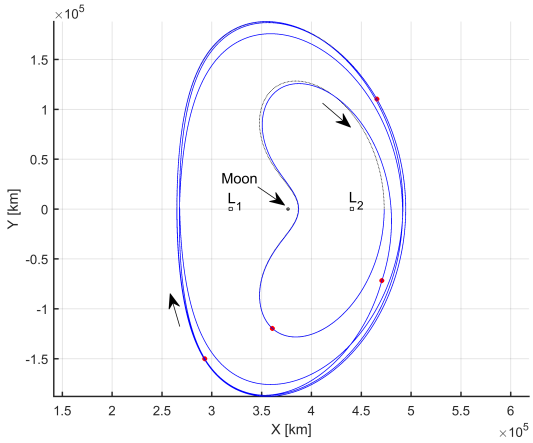

(a) An impulsive transfer derived from a low-thrust transfer similar to Figure 4(a) that uses a period-three DRO as an inermediate arc.

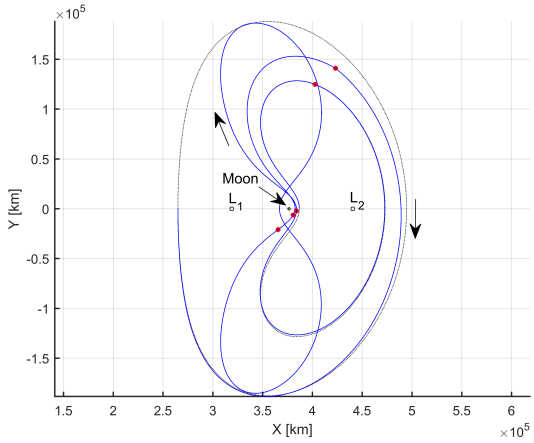

(b) An impulsive transfer derived from a low-thrust transfer similar to Figure 4(b) that uses a distant prograde orbit as an inermediate arc.

Fig. 12 Impulsive transfer solutions from an L_2 Lyapunov orbit to a DRO using optimal low-thrust transfer solutions similar to Figure 4, but with $T_{max} = 1\ N$, as the initial guesses for the multiple shooting scheme.

maneuvers. As listed in the table, the total Δv cost for this transfer is 288.1 m/s and the time of flight is 121.46 days. Note that Lantoine [11] computes transfers in an ephemeris model between the same NRHO and DRO used here and obtains Δv values from of 48 to 85 m/s, however, the transfers in that investigation generally require more than double the time of flight required for the transfer displayed in Figure 13.

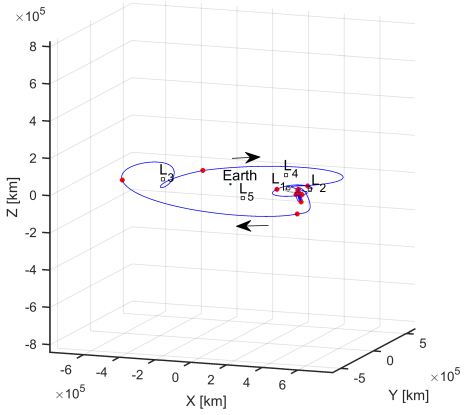

(a) Impulsive transfer in the Earth-Moon rotating frame.

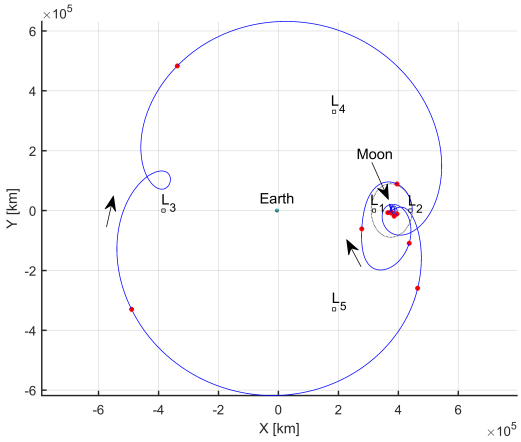

(b) Two-dimensional projection of the transfer onto the Earth-Moon rotating XY-plane.

Fig. 13 An impulsive transfer from a 9:2 NRHO to a DRO utilizing a 2:3 resonant orbit as an intermediate arc; transitioned from an optimal low-thrust solution similar to Figure 5(c), but with $T_{max} = 0.5\ N$, as the initial guess for the multiple shooting scheme.

B. Impulsive Initial Guess to Construct Low-Thrust Transfer

The orbit chain approach is a useful strategy for constructing low-thrust and impulsive transfers, however, it is only one approach for generating such paths. Other strategies for designing transfers, particularly for high-thrust spacecraft, may yield trajectories that can also serve as initial guesses for low-thrust trajectories, as well as the more

Table 4 Impulsive transfers constructed from low-thrust solutions generated via orbit chains.

Transfer Type	TOF $(days)$	Δv (m/s)
L_2 Lyapunov $\rightarrow 6 \times L_2$ Axial $\rightarrow L_2$ Vertical	151.86	475.7
NRHO $\rightarrow 12 \times L_2$ Halo $\rightarrow L_2$ Halo	163.57	264.5
L_2 Lyapunov $\rightarrow$ P3DRO $\rightarrow$ DRO	74.69	146.3
L_2 Lyapunov $\rightarrow$ DPO $\rightarrow$ DRO	94.3	128.5
NRHO $\rightarrow$ 2:3 Resonant $\rightarrow$ DRO	121.46	288.1

familiar use of impulsive solutions. Some design strategies for high-thrust spacecraft can yield trajectories with significantly different geometries than those produced via an orbit chaining approach; leveraging any novel geometries for low-thrust trajectories is also potentially beneficial. Therefore, an approach for transitioning impulsive trajectories into the low-thrust regime is necessary. The direct transcription algorithm employed in this investigation is suitable for converging impulsive trajectory solutions into low-thrust trajectories even when relatively large Δv maneuvers are included in the initial guess. The COLT algorithm is utilized to demonstrate the transition of the impulsive trajectories to feasible low-thrust paths. Note that the low-thrust trajectories described below are not optimized.

Two different impulsive transfers are employed in the next example to yield low-thrust solutions from an NRHO ($J = 3.0347$) with $r_p = 5,618.11\ km$ to a large DRO ($J = 2.6655$) with $r_p = 200,246.69\ km$; different approaches for generating the initial guess clearly influence the final low-thrust result. A puncture plot technique is employed to generate the first impulsive transfer [24]. A puncture plot is produced by introducing Δv maneuvers in many different directions at apolune along the NRHO, then propagating the trajectories that result from this maneuver. The intersections of these trajectories with the X-Y plane are recorded, and a puncture plot emerges when all the crossings are marked. Intersections that lie near the destination DRO and possess a relatively low Z velocity component are the best candidates as initial guesses for impulsive transfers. One of the points with these qualities is selected from the puncture plot and its associated trajectory is employed as an initial guess to generate the impulsive transfer displayed in Figure 14(a). This transfer is constrained to include a total of three maneuvers, two at departure and arrival, as well as one midcourse plane-change maneuver. Moreover, the arrival maneuver is required to be tangential relative to the velocity vector in the rotating frame. Key parameters associated with this transfer are summarized in Table 5. Next, the impulsive transfer that results from this design process is employed as an initial guess for a low-thrust transfer between the same two orbits, and the converged feasible result is plotted in Figure 14(b). The resulting low-thrust transfer maintains some of the shape in the initial guess, i.e., the path includes a revolution about the Earth before returning to insert onto the DRO. However, the geometry of the low-thrust transfer is significantly distorted; the path around the Earth extends much farther in the negative X direction than the initial guess, and the final segment of the trajectory completes nearly a full loop along the DRO prior to insertion. This alteration of the transfer geometry, in addition to the long periods of thrusting along the trajectory, are necessary to achieve convergence given the large velocity discontinuities at the impulsive maneuver locations in the initial guess.

A second impulsive transfer with a significantly altered geometry is designed by employing a manifold from a P3DRO in an initial guess for the transfer between the same NRHO and DRO. The resulting high-thrust trajectory, in Figure 15(a), largely follows the path of the P3DRO manifold, however, it is adjusted at the ends to accommodate the departure from the NRHO and insertion onto the DRO. A corresponding low-thrust trajectory is computed using this impulsive transfer as an initial guess, and the converged result appears in Figure 15(b). Once again, the resulting trajectory shares some characteristics with its impulsive counterpart, however, the geometry notably differs, perhaps suggesting that an impulsive initial guess is not the most useful approach. While some of the looping structure of the initial guess is preserved, these structures are shifted significantly out-of-plane to accommodate the large velocity discontinuities in the initial guess. When this out-of plane behavior is projected onto the X-Y plane, as displayed in Figure 15(b), the path appears to include a significant velocity discontinuity, however, the trajectory at this segment is, in fact, still smooth. Overall, these results demonstrate that direct transcription is able to compute low-thrust trajectories from impulsive solutions. However, more investigation is necessary to develop a process by which impulsive solutions may be more gradually transitioned to low-thrust paths to achieve more practical low-thrust results. Optimization can reduce the cost as well.

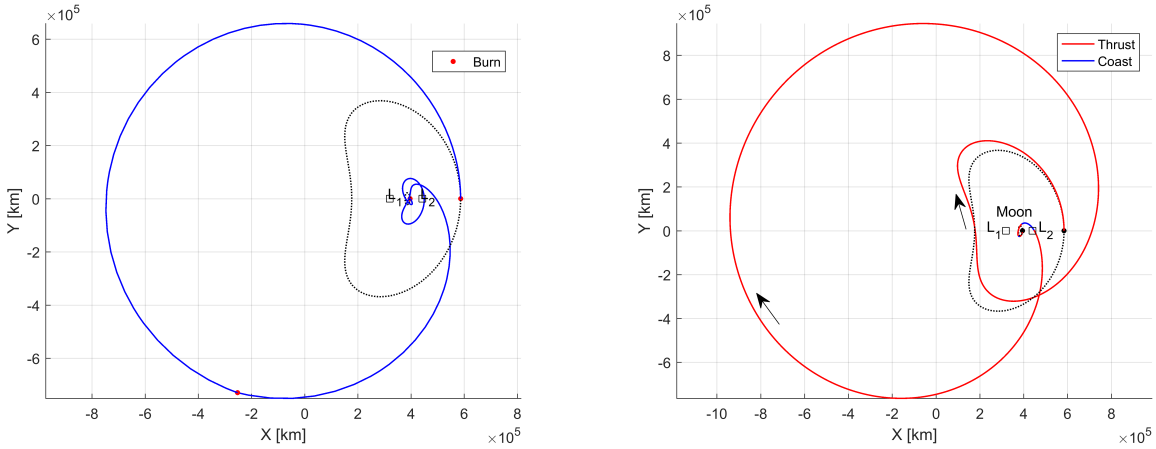

(a) Impulsive Transfer (b) Low-Thrust Transfer

Fig. 14 Impulsive transfer from a NRHO to a DRO using a puncture plot technique in 14(a) yields the low-thrust transfer plotted in 14(b). The low-thrust transfer is for a spacecraft with $m_0 = 1000\ kg$, $T_{max} = 200\ mN$, and $I_{sp} = 2000\ sec$.

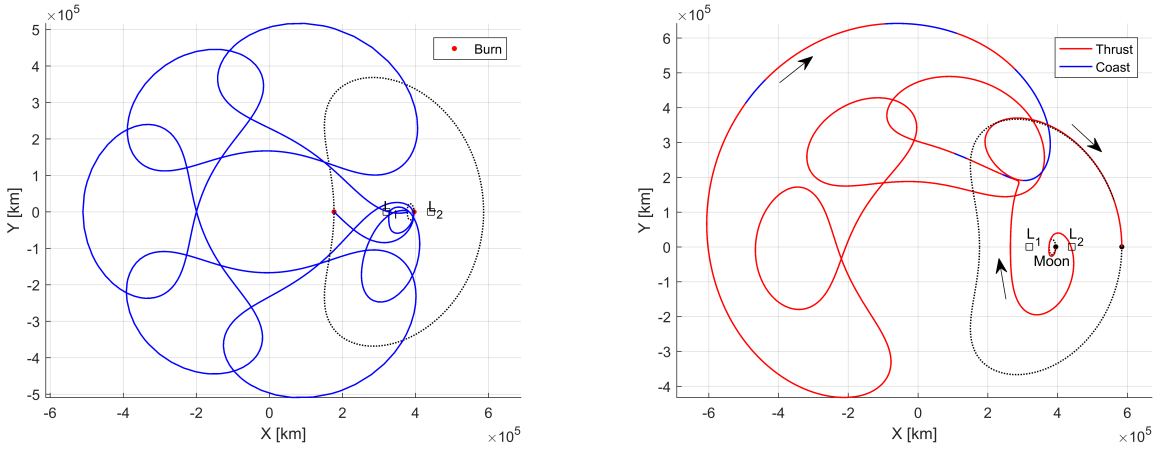

(a) Impulsive Transfer (b) Low-Thrust Transfer

Fig. 15 Impulsive transfer from a 9:2 synodic resonance NRHO to a DRO obtained using a manifold from a period three DRO in the initial guess in 15(a), and the low-thrust transfer that results when the impulsive transfer is employed as an initial guess in 15(b). The low-thrust transfer is for a spacecraft with $m_0 = 1000\ kg$, $T_{max} = 200\ mN$, and $I_{sp} = 2000\ sec$.

Table 5 Low-thrust transfers constructed from impulsive solutions and examined for a spacecraft with $m_0 = 1000\ kg$, $T_{max} = 200\ mN$, and $I_{sp} = 2000\ sec$.

Transfer Type	$TOF\ (days)$	$\Delta m\ (kg)$	m_f/m_0	$\Delta v\ (m/s)$
Impulsive: NRHO → DRO (from puncture plot)	167.6952	NA	NA	1,474.3249
Impulsive: NRHO → DRO (with P3DRO manifold)	73.3427	NA	NA	713.5267
LT: NRHO → DRO (from puncture plot)	167.6952	131.9979	0.8680	2,776.4804
LT: NRHO → DRO (with P3DRO manifold)	73.3427	59.9116	0.9401	1,211.7358

C. Transition to Ephemeris Model

A subset of the impulsive trajectories computed in this investigation are selected for transition to an ephemeris model to test their feasibility within a higher fidelity regime. Specifically, the N-body equations of motions in Equation 5 are employed along with the JPL DE421 ephemerides to converge the impulsive trajectories displayed in Figures 12, 10, and 13 (originally computed in the CR3BP using low-thrust solutions as an initial guess) within the Earth, Moon, Sun, and Jupiter ephemeris model. A variable time multiple shooting scheme is employed to correct the impulsive trajectories in the ephemeris model, and the resulting paths are displayed in Figures 16 and 17. Note that the initial and final points along the paths that appear in Figures 16 and 17 are derived from states in the original CR3BP transfer that were transformed to the inertial frame. The trajectories are constrained to originate and terminate at these points. Since the initial and final states along the path do not necessarily correspond to states on ephemeris versions of the departure and arrival orbits, respectively, the transition of these trajectories from the CR3BP to the ephemeris model serves to illustrate that the geometry of the CR3BP solution is maintained within a higher fidelity model and offers a step towards producing end-to-end transfer designs within this regime. Note that low-thrust transfers in the ephemeris model, similar to those included in this study and computed with the same techniques, are converged in an ephemeris model by Pritchett, Grebow, and Howell [12].

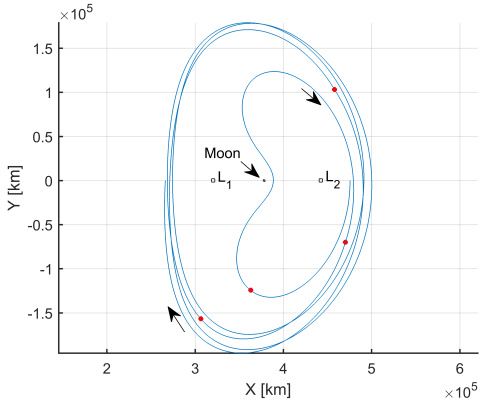

(a) Impulsive path in ephemeris model from Figure 12(a)

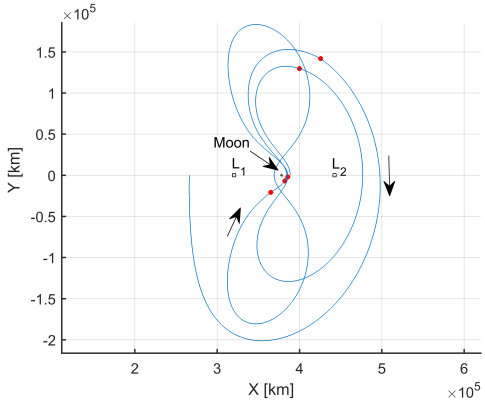

(b) Impulsive Path in ephemeris model from Figure 12(b)

Fig. 16 Impulsive paths in an ephemeris model obtained using the CR3B model impulsive transfers in Figures 12(a) and 12(b) as initial guesses.

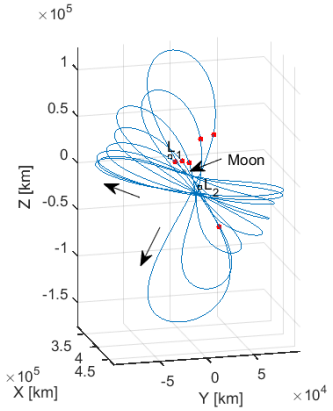

(a) Impulsive Path in ephemeris model from Figure 11(b)

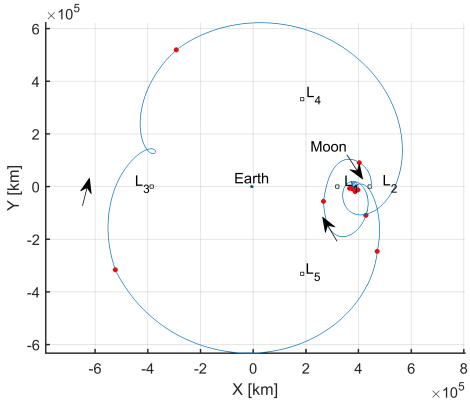

(b) Impulsive Path in ephemeris model from Figure 14

Fig. 17 Impulsive paths in an ephemeris model obtained using the CR3B model impulsive transfers in Figures 10(b) and 13 as initial guesses.

VI. Concluding Remarks

The investigation expands upon a trajectory design approach that leverages a robust direct transcription algorithm to generate transfers between periodic orbits in the CR3BP using chains of natural dynamical structures available in this model. Many different natural dynamical structures are utilized including libration point orbits, resonant orbits, and manifold segments. Each type of structure in an orbit chain comprises a link; any number of links may be included and individual links can be duplicated to yield multiple revolutions. Thus, orbit chains of arbitrary size and times of flight are formed. While the direct transcription algorithm that is employed to converge orbit chains into continuous transfers is robust, some orbit chain itineraries are more likely to deliver local optimal solutions that are less desirable.

In addition to optimal low-thrust transfers, the orbit chaining technique is suitable for formulating initial guesses for impulsive transfers. With this approach, the direct transcription algorithm is applied to an orbit chain using a high value of maximum thrust. This formulation frequently yields a continuous trajectory with brief periods of thrusting, similar to the instantaneous burns in impulsive solutions. This trajectory is then easily transitioned to an impulsive solution that retains much of the same geometry as the low-thrust initial guess, as well as a total Δv of the same order of magnitude. Finally, the direct transcription algorithm employed to correct orbit chains is also applicable to the task of transitioning impulsive transfer trajectories to low-thrust solutions. However, impulsive transfer solutions with lower Δv magnitudes likely yield low-thrust solutions that more closely resemble an impulsive initial guess.

Overall, the techniques explored are straightforward approaches to the challenging process of trajectory transfer design. These techniques are particularly suitable for transfer design between stable or nearly stable periodic orbits because these orbits do not possess unstable invariant manifold structures that can assist in transfer concept development. Future efforts are focused on efficient strategies for the selection of appropriate links in an orbit chain. Reliable strategies for selecting the links in an orbit chain, as well as "recipes" for common transfer design scenarios, will be advantageous for the long-term implementation of an orbit chaining approach. Finally, the interchange between low-thrust and impulsive solutions, can yield novel geometries and a wider range of transfer concepts.

Acknowledgments

Gratitude must be extended to Ashwati Das-Stuart, Bonnie Prado, Daniel Grebow, and Thomas Pavlak, for beneficial conversations and suggestions. This work was conducted at Purdue University and is supported in part by the NASA Space Technology Research Fellowship, NASA Grant No. NNX16AM42H, as well as support from Johnson Space Center under Grant No. NNX13AK60A.

References

[1] Whitley, R., Martinez, R., Condon, G., Williams, J., and Lee, D., "Cislunar Near Rectilinear Halo Orbits for Human Space Exploration," *AIAA Space*, 2016.

[2] Kutter, B. F., and Sowers, G. F., "Cislunar-1000: Transportation supporting a self-sustaining Space Economy," *AIAA SPACE 2016*, No. 1 in AIAA SPACE Forum, AIAA, Long Beach, California, 2016, pp. 1–14. doi:10.2514/6.2016-5491.

[3] Minghu, T., Ke, Z., Meibo, L., and Chao, X., "Transfer to long term distant retrograde orbits around the Moon," *Acta Astronautica*, Vol. 98, No. 1, 2014, pp. 50–63. doi:10.1016/j.actaastro.2014.01.016.

[4] Capdevila, L., Guzzetti, D., and Howell, K. C., "Various Transfer Options from Earth into Distant Retrograde Orbits in the Vicinity of the Moon," *Advances in the Astronautical Sciences*, Vol. 152, No. 1, 2014, pp. 3659–3678.

[5] Welch, C. M., Parker, J. S., and Buxton, C., "Mission Considerations for Transfers to a Distant Retrograde Orbit," *Journal of the Astronautical Sciences*, Vol. 62, No. 2, 2015, pp. 101–124. doi:10.1007/s40295-015-0039-z.

[6] Whitley, R., Martinez, R., Condon, G., Williams, J., and Lee, D., "Targeting Cislunar Near Rectilinear Halo Orbits for Human Space Exploration," *AAS/AIAA Astrodynamics Specialist Conference Space*, 2017, pp. 1–20.

[7] Capdevila, L., "A Transfer Network Linking Earth, Moon and the Libration Point Regions in the Earth-Moon System," Ph.D. Dissertation, Purdue University, West Lafayette, Indiana, 2016.

[8] Parker, J. S., Bezrouk, C., and Davis, K. E., "Low-Energy Transfers to Distant Retrograde Orbits," *Advances in the Astronautical Sciences Spaceflight Mechanics*, Vol. 155, 2015, pp. 1–15.

[9] Herman, J. F. C., "Improved Collocation Methods to Optimize Low-Thrust , Low-Energy Transfers in the Earth-Moon System by," Ph.D. Thesis, University of Colorado, Boulder, Colorado, 2015.

[10] Parrish, N. L., Parker, J. S., Hughes, S. P., and Heiligers, J., "Low-Thrust Transfers From Distant Retrograde Orbits To L2 Halo Orbits in the Earth-Moon System," *International Conference on Astrodynamics Tools and Techniques*, Darmstadt, Germany, 2016, pp. 1–9.

[11] Lantoine, G., "Efficient NRHO to DRO Transfers in Cislunar Space," *AAS/AIAA Astrodynamics Specialist Conference*, Stevenson, Washington, 2017, pp. 1–18.

[12] Pritchett, R. E., Howell, K. C., and Grebow, D. J., "Low-Thrust Transfer Design Based on Collocation Techniques: Applications in the Restricted Three-Body Problem," *AAS/AIAA Astrodynamics Specialist Conference*, Stevenson, Washington, 2017, pp. 1–20.

[13] Gerstenmaier, W. H., "Progress in Defining the Deep Space Gateway and Transport Plan," Tech. rep., NASA, March 28, 2017. URL `https://www.nasa.gov/sites/default/files/atoms/files/nss_chart_v23.pdf`.

[14] Hambleton, K., "Deep Space Gateway to Open Opportunities for Distant Destinations," , March 28, 2017. URL `https://www.nasa.gov/feature/deep-space-gateway-to-open-opportunities-for-distant-destinations`.

[15] Rayman, M. D., Varghese, P., Lehman, D. H., and Livesay, L. L., "Results from the Deep Space 1 Technology Validation Mission," *Acta Astronautica*, Vol. 47, 2000, p. 3 & 8.

[16] Russell, C., and Raymond, C. (eds.), *The Dawn Mission to Minor Planets 4 Vesta and 1 Ceres*, New York, 2012.

[17] Kuninaka, H., Nishiyama, K., Shimizu, Y., Funaki, I., Koizumi, H., Hosoda, S., and Nakata, D., "Hayabusa Asteroid Explorer Powered by Ion Engines on the way to Earth," *31st International Electric Propulsion Conference*, 2009, p. 2.

[18] Betts, J. T., "Survey of Numerical Methods for Trajectory Optimization," *Journal of Guidance, Control, and Dynamics*, Vol. 21, No. 2, 1997, pp. 193–207.

[19] Topputo, F., and Zhang, C., "Survey of Direct Transcription for Low-Thrust Space Trajectory Optimization with Applications," *Abstract and Applied Analysis*, Vol. 2014, 2014, p. 15.

[20] Ozimek, M. T., Grebow, D. J., and Howell, K. C., "A Collocation Approach for Computing Solar Sail Lunar Pole-Sitter Orbits," *Open Aerospace Engineering Journal*, Vol. 3, 2010, pp. 65–75. doi:10.2174/1874146001003010065.

[21] Grebow, D. J., and Pavlak, T. A., "MColl: Monte Collocation Trajectory Design Tool," *AAS/AIAA Astrodynamics Specialist Conference*, Stevenson, Washington, 2017, pp. AAS 17–776.

[22] Gill, P. E., Murray, W., and Saunders, M. A., "SNOPT: An SQP Algorithm for Large-Scale Constrained Optimization," *SIAM Journal on Optimization*, Vol. 12, No. 4, 2002, pp. 979–1006. doi:10.1137/S1052623499350013.

[23] Gill, P. E., Murray, W., Saunders, M. A., and Wong, E., "User's Guide for SNOPT 7.6: Software for Large-Scale Nonlinear Programming," Center for Computational Mathematics Report CCoM 17-1, Department of Mathematics, University of California, San Diego, La Jolla, CA, 2017.

[24] Zimovan, E., "Characteristics and Design Strategies for Near Rectilinear Halo Orbits within the Earth-Moon System," M.S. Thesis, Purdue University, West Lafayette, Indiana, 2017.

[25] Barden, B., Howell, K., and Lo, M. W., "Application of Dynamical Systems Theory to Trajectory Design for a Libration Point Mission," *AIAA/AAS Astrodynamics Specialist Conference*, American Institute of Aeronautics and Astronautics, Inc., San Diego, California, 1996, pp. 1–14.

[26] Howell, K. C., Barden, B. T., and Lo, M. W., "Application of Dynamical Systems Theory to Trajectory Design for a Libration Point Mission," *The Journal of the Astronautical Sciences*, Vol. 45, No. 2, 1997, pp. 161–178.

[27] Koon, W. S., Lo, M. W., Marsden, J. E., and Ross, S. D., "Heteroclinic connections between periodic orbits and resonance transitions in celestial mechanics," *Chaos: An Interdisciplinary Journal of Nonlinear Science*, Vol. 10, No. 2, 2000, pp. 427–469. doi:10.1063/1.166509.

[28] Gómez, G., Koon, W. S., Lo, M. W., Marsden, J. E., Masdemont, J. J., and Ross, S. D., "Connecting orbits and invariant manifolds in the spatial restricted three-body problem," *Nonlinearity*, Vol. 17, No. 5, 2004, pp. 1571–1606. doi:10.1088/0951-7715/17/5/002.

[29] Vaquero, M., and Howell, K. C., "Leveraging Resonant-Orbit Manifolds to Design Transfers Between Libration-Point Orbits," *Journal of Guidance, Control, and Dynamics*, Vol. 37, No. 4, 2014, pp. 1143–1157. doi:10.2514/1.62230.

[30] Restrepo, R. L., and Russell, R. P., "Patched Periodic Orbits: A Systematic Strategy for Low Energy Transfer Design," *AAS Astrodynamics Specialists Conference*, 2017, pp. 1–20.

[31] Haapala, A. F., and Howell, K. C., "A Framework for Constructing Transfers Linking Periodic Libration Point Orbits in the Spatial Circular Restricted Three-Body Problem," *International Journal of Bifurcation and Chaos*, Vol. 26, No. 05, 2016, p. 1630013. doi:10.1142/S0218127416300135.